Characteristics Mode Analysis of a Unit-Cell and A 3×3 Finite Metasurface Design for IoT Applications in the mm-wave Band

Ubaid Ullah
Networks and Communication Engineering Department
Al Ain University,
P.O. Box (112612), Abu Dhabi, UAE.
ubaid.ullah@aau.ac.ae

Slawomir Koziel
Engineering Optimization and Modeling Center of Reykjavik University, Reykjavik, Iceland
koziel@ru.is

Anna Pietrenko-Dabrowska
Faculty of Electronics, Telecommunications and Informatics, Gdansk University of Technology, 80-233 Gdansk, Poland
anna.dabrowska@pg.edu.pl

Shahanawaz Kamal
Radio Frequency Design Enablement Group, Barkhausen Institut, 01067 Dresden, Germany
shahanawaz.kamal@barkhauseninstitut.org

***Abstract*—This paper presents a characteristic mode analysis of a novel metasurface (MTS) for the applications related to the Internet of Things (IoT) at millimeter-wave (mm-wave) band. The CMA is utilized to investigate different modes within the unit-cell design of the proposed metasurface. Through comprehensive analysis, two orthogonal TM modes exhibiting a broadside radiation pattern were identified. These modes were then simultaneously excited on a single substrate using straightforward coplanar waveguide (CPW) magnetic dipoles, resulting in circular polarization (CP). Additionally, it has been shown that the sense of polarization can be easily reconfigured, enabling the realization of a multiple-input-multiple-output (MIMO) antenna implemented with polarization diversity. Mode analysis of the unite cell design is performed followed by a 3×3 implementation of the metasurface (MTS). A number of modes and their radiation pattern of the unit-cell and the MTS are analyzed using CMA. The two orthogonal modes with broadside radiation and modal significance (MS) close to unity are then excited using a coplanar waveguide feeding on a single substrate. The numerical analysis of the design exhibits wide impedance bandwidth from 23 GHz to 30 GHz. The 3 dB axial ratio (AR) of the proposed antenna is from 25.3 GHz to 30 GHz with the peak gain of 7.4 dBic in the broadside direction.**

Keywords*—*unit-cell design, metasurface, mm-wave band, planar designs, circular polarization

I. Introduction

The forthcoming wireless communication systems demands for higher data rates for sustainable connectivity and data flow. These technologies include the fifth and sixth generation, the Internet of Things (IoT), and other well-known RF fields. To meet the high data-rate requirement of the forthcoming technologies, migration to the higher mm-wave frequencies is indispensable [1]-[3]. The scarcely used mm-wave band offers wideband and high data rates opportunities, but on the other hand in long-distance mm-wave communication suffers from propagation losses and multipath effects leading to unstable communication. In long distance wireless communication, electromagnetic waves propagate through multiple mediums and through extended air medium, increasing the likelihood of signal obstruction by physical obstacles such as walls, trees, and buildings. For linearly polarized waves, this can result in significant data signal loss due to severe multipath effects and signal interference, particularly in urban areas [4], [5]. In such scenarios, circular polarization (CP) is advantageous as it reduces multipath effects, absorption losses, signal interference, and signal attenuation, thereby maintaining signal integrity.

Designing a high-performance, wideband CP antenna is challenging, as CP structures require a sophisticated feeding circuit to generate two orthogonal vector fields of the same magnitude [6]. One straightforward method to achieve CP is using a single-feed microstrip antenna [7], [8]. However, this typically results in a narrow 3 dB axial ratio (AR) bandwidth of about 1.5% due to the excitation of only one mode. Various approaches have been proposed to improve the AR bandwidth, including multi-point feeding methods that achieve wideband performance but require complex feeding networks compared to single-feed methods [8]-[10]. Consequently, there is considerable interest in enhancing single-feed antenna designs to improve AR and impedance bandwidth [11], [12]. The electrical characteristics, especially AR, are sensitive to the geometrical dimensions of the feeding structure, and even minor alterations can degrade performance. Therefore, simplifying the antenna's geometry and excitation circuit would improve circuit precision and fabrication yield. Metasurface (MTS)-based antennas utilize the resonant modes of a finite MTS for radiation, featuring low profiles, wide bandwidth, and easy implementation. Various MTS antennas have been proposed to meet specific requirements, including compact size, wideband capability, circular polarization, and low-profile applications [13]-[18]. Characteristic mode analysis (CMA) has proven effective in predicting the modal behaviors of metasurfaces, providing valuable insights into these antennas [19]-[23]. By precisely adjusting the desired modes using CMA, the characteristics of metasurfaces can be optimized [24]. Although CMA has not been widely used for broadband CP MTS antennas, its potential remains significant. A few designs based on CMA analysis have achieved wideband characteristics, but they often involve multilayer implementations with shorting pins for the feeding network or result in linear polarization or narrow bandwidth [24]-[27]. Only a limited number of single-layer MTS antennas have achieved wideband CP radiation while maintaining a low profile [23], [24].

This paper presents a single-layer MTS-based wideband CP antenna for the mm-wave band. It introduces a new octagonal star-shaped unit cell and performs its modal analysis using CMA. Two orthogonal modes with broadside radiation and modal significance (MS) close to unity are identified. A CMA analysis of a 3×3 MTS ensures mode consistency. Simultaneous excitation of these modes results in CP, achieved by utilizing a coplanar waveguide feeding in combination with magnetic dipoles created by narrow slots. The design is executed on a single substrate, ensuring a compact, low-profile antenna. Numerical analysis shows a wide reflection coefficient from 25 GHz to 30.8 GHz. The antenna's 3 dB AR bandwidth ranges from 26 GHz to 31 GHz, with a peak gain of 7.4 dBic in the broadside direction. The main benefits of this research contribution include: (i) development of a new unit cell and its uniform MTS design; (ii) achieving CP using a simple feeding technique on a single substrate; (iii) demonstrating polarization reconfiguration by simple feed alteration; (iv) achieving wideband operation in terms of impedance and AR bandwidth, with a stable directional pattern and low mutual coupling; (v) realizing these performance metrics with a low-profile, easy-to-fabricate antenna structure

II. Metasurface Design And Analysis Using CMA

A unit-cell design and its respective 3×3 MTS of the proposed metasurface with its geometrical parameters are shown in Fig. 1. The unit-cell design has two metallic patches stacked diagonally on top of each other, forming an octagonal star shape structure. The first four modes of the unit cell are studied using CMA analysis, although only two orthogonal modes are selected for the proposed design. The modal significance of the chosen modes is shown in Fig. 2. The modal significance of the proposed MTS refers to the importance or contribution of each mode in the overall behavior and performance of the antenna. It indicates how much each mode contributes to the antenna's functionality, radiation characteristics, and polarization. A higher modal significance suggests that the corresponding mode plays a more dominant role in shaping the antenna's behavior. Note that a mode is resonant when MS = 1 whereas it is non-resonant when its MS = 0. As $MS \geq 1/\sqrt{2}$ offers more effective radiation, therefore, a reference line is used at 0.707 to indicate that region [4] [23]. Figure 2 clearly shows that the resonant frequencies of both modes are near 28 GHz. CMA's dependence on frequency is a well-known factor [19], leading to variations in both modal current and modal radiation pattern. Hence, the vector fields of the two modes (mode 1 and mode 2) of the unit cell is shown at multiple frequencies; i.e. 27 GHz, 28 GHz, and 29 GHz in Fig. 3. The figure reveals that both modes maintain a consistent modal current distribution across the frequency spectrum. Moreover, the surface current visibly shows the phase difference between the two modes at all the frequency points. This has been further clarified with the vector lines pointed in the direction of the maximum current, as illustrated in Fig. 4. These vector lines depict the distinct directions of the electric field vectors for each mode, confirming their orthogonal nature. This orthogonality is crucial for achieving circular polarization when both modes are simultaneously excited. The combined vectors show orthogonal field configuration of the modes with the peak current components for mode 1 along $M_{1(x,y)}$ and mode 2 along $M_{2(-x,y)}$. The orientation of the vector fields depicted in Fig. 4 offers substantial empirical evidence affirming the existence of orthogonal modes. Similarly, the 3D radiation pattern of both modes is illustrated in Fig. 5 at the same frequencies. It is seen that both modes are radiating energy in the broadside direction at all frequencies. Therefore, simultaneous excitation of these modes results in the CP antenna with broadside radiation.

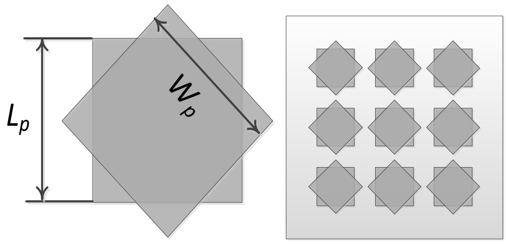

Fig. 1. The proposed metasurface design consists of the following components: (a) Unit-cell: This represents the basic building block of the metasurface, (b) 3×3 MTS: This is a 3×3 array of the unit cells, forming the complete metasurface structure.

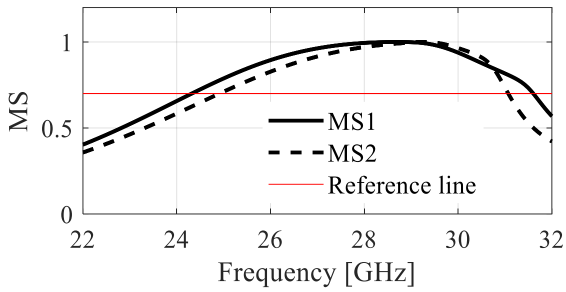

Fig. 2. Modal significance of the proposed MTS.

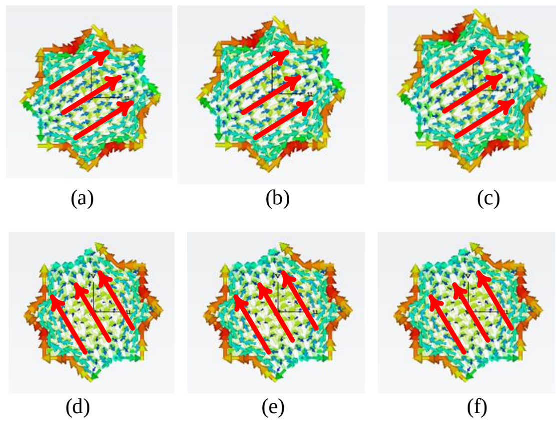

Fig. 3. The surface current distribution of the modes at different frequencies is shown below: Mode 1: (a) Mode 1 ssurface current at 27 GHz, (b) Mode 1 surface current at 28 GHz, (c) Mode 1 ssurface current at 29 GHz, (d) Mode 2 surface current at 27 GHz, (e) Mode 2 Surface current at 28 GHz, (f) Mode 2 surface current at 29 GHz

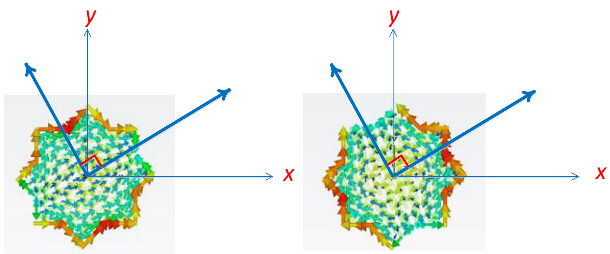

Fig. 4. The orthogonality of the modes is illustrated using vector lines.

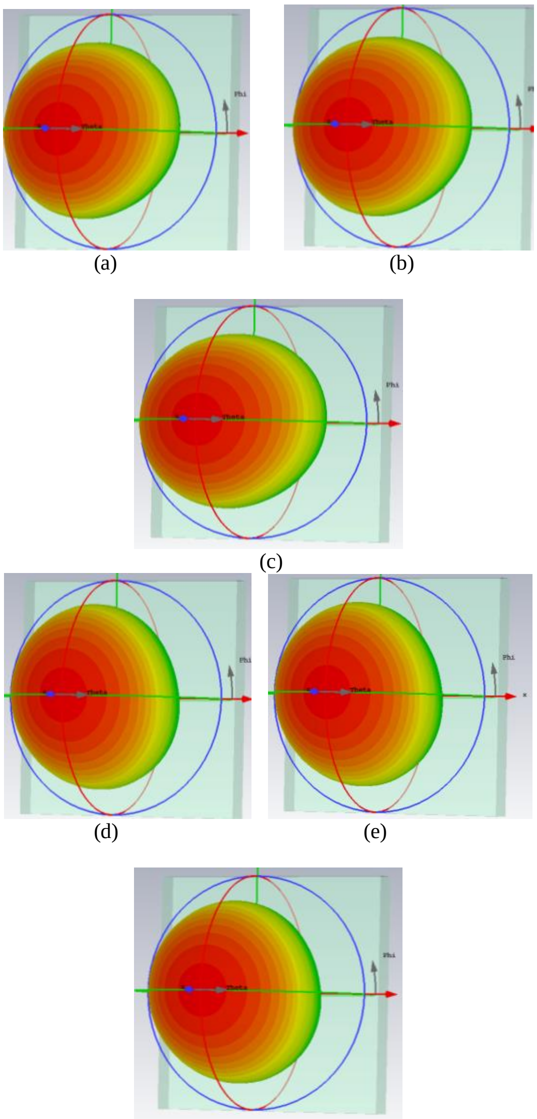

Fig. 5. The radiation pattern of the two selected modes is presented as follows: Mode 1: (a) Mode 1 at 27 GHz, (b) Mode 1 at 28 GHz, (c) Mode 1 at 29 GHz, Mode 2: (d) Mode 2 at 27 GHz, (e) Mode 2 at 28 GHz (f) Mode 2 at 29 GHz.

III. Antenna Design And Analysis

A. Antenna Design

The proposed design utilizes a single Rogers RO4003 substrate, characterized by a dielectric permittivity (εr) of 3.38 and a thickness of 0.813 millimeters (mm). Atop this substrate, a 50-ohm coplanar waveguide (CPW) feed is established, flanked by two narrow slots on either side to generate a magnetic current source. The gap between the feed line and the coplanar ground plane is fixed at 0.313 mm, while the width of the feed line measures 1.05 mm.

Illustrations of the antenna's geometry are provided in Figure 6. Figure 6(a) showcases the front view of the feeding configuration, while Figure 6(b) displays the 3×3 metasurface (MTS) installed at the substrate's rear. Moreover, Figure 6(c) presents a detailed depiction of the parameterized slot geometry. These slot dimensions are optimized concurrently with the MTS radiator. Positioning the current sources strategically ensures effective excitation of the two orthogonal modes, locating them where the magnetic field strength of the modes is maximal. Parameter "d" (shown in Figure 6(b)) denotes the distance from the port to the center of the MTS, a crucial factor in aligning the MTS over the magnetic current for optimal energy coupling. To prevent radiation from the feed line within the operating band, the open end of the microstrip line is linked to the coplanar ground. Employing a multi-stage optimization process at the full-wave level, all geometrical parameters of the antenna are fine-tuned. The resulting optimum parameters are detailed in Table 1.

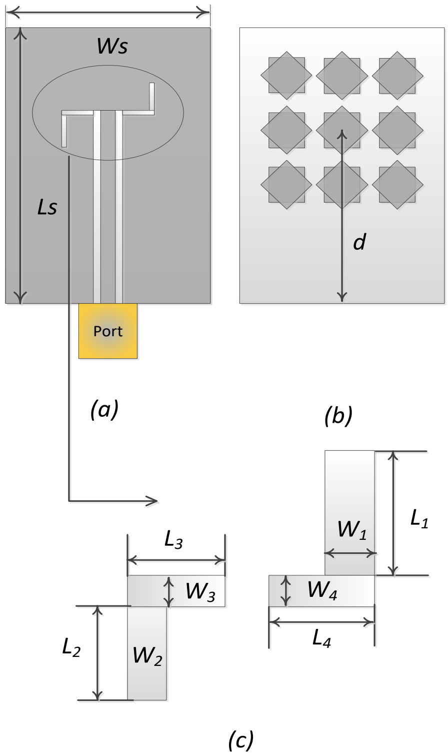

Fig. 6. The structure and geometry of the proposed single-layer MTS-based antenna are illustrated as follows: (a) Coplanar Waveguide (Top View), (b) 3×3 MTS (Back View), (c) Enlarged Parameterized Slots (Magnetic Dipoles).

B. Operational Framework and Circular Polarization

The operational principle of the proposed MTS-based antenna is simple to understand. Figures 3 and 5 display the surface current of the two chosen modes derived from the unit cell design, along with their associated radiation patterns. To deepen our comprehension of the entire MTS, we examine the modal electric near field alongside the current distribution. As depicted in Figures 7 and 8, the current distribution of the two modes across the 3×3 MTS and their resulting far-field patterns at two frequency points are showcased. These figures clearly illustrate that the MTS maintains the modal behavior observed in the unit cell, along with the radiation pattern directed towards the broadside. Additionally, the radiation patterns of the MTS closely align with those of the unit cell in the far-fields. The excitation of the two orthogonal modes, identified through CMA analysis, is facilitated by the magnetic dipole currents generated by the CPW slots.

The selection of the feeding mechanism aims to excite the two modes by employing two electric field components with perpendicular polarizations linked to the aperture. This approach entails adjusting the position of the MTS relative to the feed line to ensure that the maximum current aligns precisely with the magnetic current of the slot, thus optimizing energy coupling to the MTS. An examination of Fig. 3 and

Fig. 7 reveals that the maximum modal currents are concentrated not only on the edges of the unit cell but also on the finite MTS. Consequently, L-shaped slots are strategically designed to facilitate maximum energy coupling to the radiator. This method effectively stimulates both orthogonal modes, resulting in the generation of left-hand circular polarization (LHCP). It is remarkable that this feeding technique feature multiple advantages that includes a low-profile planar design, cost-effectiveness, and geometrical simplicity, as it printed on a single substrate. This restructured design improves the overall efficiency and practicality of the proposed antenna system, making it appropriate for a wide range of applications in modern wireless communication.

TABLE I. ANTENNA'S PHYSICAL PARAMETRS

Parameter	Value	Parameter	Value	Parameter	Value
L_s	21.999	L_2	3.5567	W_4	0.4030
W_s	14.598	W_2	0.6705	L_p	2.0894
D	15.360	L_3	2.2179	W_p	1.9024
L_1	3.7622	W_3	0.2053	W_m	1.0500
W_1	0.5667	L_4	1.9358	L_m	13.7667

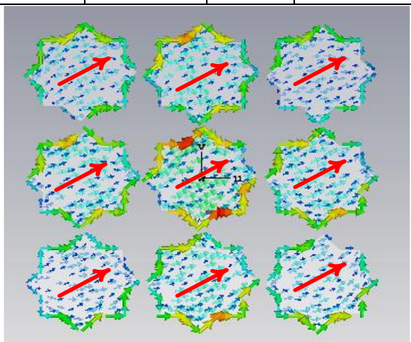

(a)

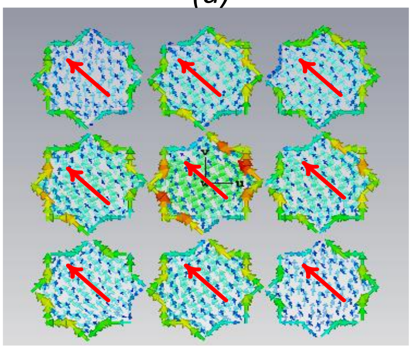

(b)

Fig. 7. Surface currents of the modes are depicted as follows: (a) Surface current of Mode 1 on the MTS, (b) Surface current of Mode 2 on the MTS.

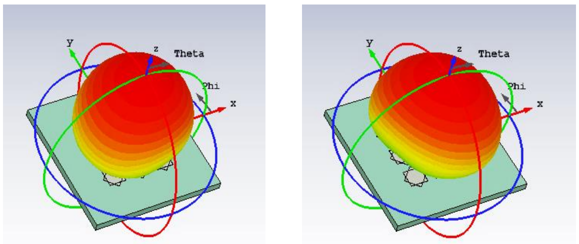

(a)

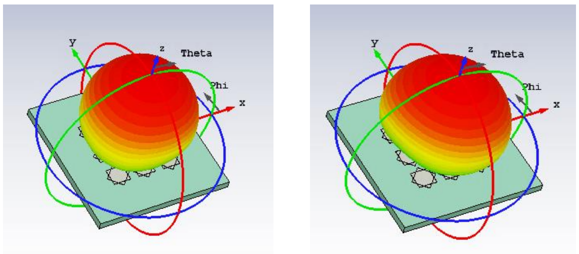

(b)

Fig. 8. The mode 1 farfiled patterns (left) and mode 2 (right) are demonstrated at two different frequencies: (a) 27 GHz, and (b) 29 GHz.

IV. Results And Discussion

The numerical evaluation of the proposed antenna, utilizing single-layer MTS technology, was performed using full-wave electromagnetic (EM) simulations. To ensure the accuracy of the results, a Southwest end-launch connector, identical to the one used in the experimental characterization, was incorporated into the numerical model. All geometric parameters of the antenna were systematically optimized through a multi-stage optimization. The simulated reflection coefficient (S_{11}) and axial ratio (AR) of the proposed MTS based antenna are illustrated in Fig. 9. The S_{11} shows a wideband response as the antenna is operational with S_{11} below -10 dB from 22.4 GHz to 30 GHz. The axial ratio of the antenna is below 3 dB reference value from 25.3 GHz to 30 GHz depicting a wideband CP performance. The realized gain (RG) of the proposed antenna is illustrated in Fig. 10. The peak realized gain of the antenna is 7.4 dBic while average in-band gain is 5.3 dBic, reflecting a consistent radiation in the boresight direction. Further to confirm the excitation of the two selected modes, the 3D radiation pattern is shown in Fig. 11 which clearly indicate broadside radiation.

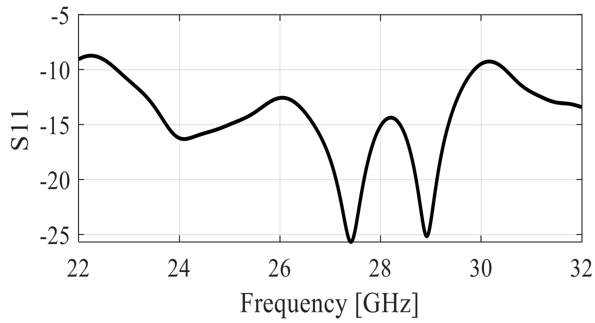

(a)

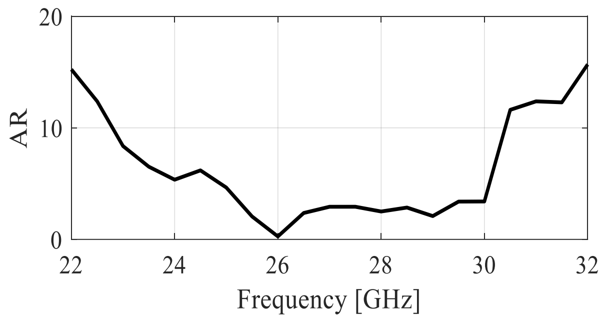

Figure 9. (a) Reflection coefficient (left) and (b) axial ratio (right) of the proposed antenna

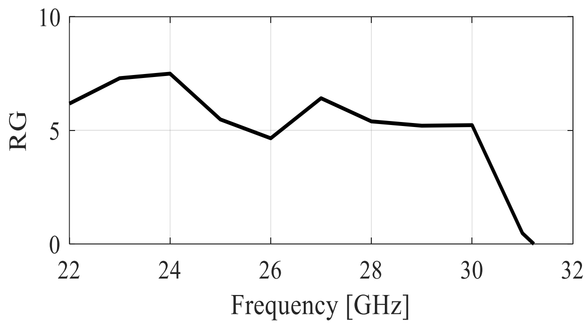

Figure 10. Realized gain of the proposed antenna

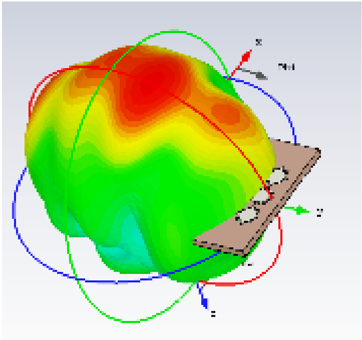

(a)

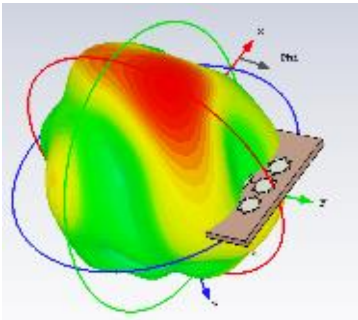

(b)

Figure 11: 3D radiation pattern of the Antenna; (a) 26 GHz, (b) 28 GHz

V. Conclusion

In this paper, we present an innovative design for a single-layer circularly polarized antenna. A single-layer antenna based on orthogonal modes of MTS is designed. CPW is used to excite the two modes simultaneously achieving a wideband CP antenna. The proposed design utilizes a new finite MTS structure, excited by a simple CPW feeding mechanism. Before implementing the antenna design, we comprehensively studied a new unit cell design using CMA to identify orthogonal modes with similar radiation characteristics. Multiple modes of the unit cell design were analyzed, and two suitable modes were identified. Following this, a 3 × 3 MTS was analyzed using CMA to ensure mode consistency within the MTS. The radiation patterns of both the unit cell design and the 3 × 3 MTS were investigated to verify their properties, particularly directivity. Subsequently, a CPW feeding mechanism was adopted to excite the MTS with magnetic dipoles created by narrow slits in the coplanar ground planes. The MTS was positioned at the back of the substrate to ensure strong coupling between the magnetic dipoles and the MTS, resulting in the simultaneous excitation of the two selected modes with broadside radiation.

References

[1] J. Wang, H. Wong, Z. Ji, and Y. Wu, "Broadband CPW-fed aperture coupled metasurface antenna," *IEEE Antennas Wireless Propag. Lett.*, vol. 18, no. 3, pp. 517–520, Mar. 2019.

[2] F. H. Lin and Z. N. Chen, "A method of suppressing higher order modes for improving radiation performance of metasurface multiport antennas using characteristic mode analysis," *IEEE Trans. Antennas Propag.*, vol. 66, no. 4, pp. 1894–1902, Apr. 2018.

[3] M. Cabedo-Fabres, E. Antonino-Daviu, A. Valero-Nogueira, and M. F. Bataller, "The theory of characteristic modes revisited: A contribution to the design of antennas for modern applications," *IEEE Antennas Propag. Mag.*, vol. 49, no. 5, pp. 52–68, Oct. 2007.

[4] X. Gao, G. Tian, Z. Shou, and S. Li, "A low-profile broadband circularly polarized patch antenna based on characteristic mode analysis," *IEEE Antennas Wireless Propag. Lett.*, vol. 20, no. 2, pp. 214–218, Feb. 2021.

[5] C. Zhao and C.-F. Wang, "Characteristic mode design of wide band circularly polarized patch antenna consisting of H-shaped unit cells," *IEEE Access*, vol. 6, pp. 25292–25299, 2018.

[6] X. Yang, Y. Liu, and S.-X. Gong, "Design of a wideband omnidirectional antenna with characteristic mode analysis," *IEEE Antennas Wireless Propag. Lett.*, vol. 17, no. 6, pp. 993–997, Jun. 2018.

[7] S. Liu, D. Yang, Y. Chen, K. Sun, X. Zhang, and Y. Xiang, "Design of single-layer broadband omnidirectional metasurface antenna under single mode resonance," *IEEE Trans. Antennas Propag.*, vol. 67, no. 5, pp. 3527–3532, May 2021.

[8] A. E. Yousfi, A. Lamkaddem, K. A. Abdalmalak, and D. S. Vargas, "Design of a broadband circularly-polarized single-layer metasurface antenna using CMA," *in Proc. 15th Eur. Conf. Antennas Propag.* (EuCAP), Dusseldorf, Germany, Mar. 2021, pp. 1–5.

[9] Z. Zhang, Y. Cheng, H. Luo, and F. Chen, "Low-Profile Wideband Circular Polarization Metasurface Antenna With Characteristic Mode Analysis and Mode Suppression," *IEEE Antennas Wireless Propag. Lett*, vol. 22, no. 4, pp. 898-902, April 2023.

[10] K. Gao, X. Cao, J. Gao, T. Li, H. Yang and S. Li, "Low-RCS metasurface antenna array design with improved radiation performance using odd- and even-mode analysis", *IEEE Antennas Wireless Propag. Lett.*, vol. 21, no. 2, pp. 421-425, Feb. 2022.

[11] X. Wei, L. He, J. Zeng, D. Fei and H. Liu, "A center-fed triple-mode wideband circularly polarized phased array using characteristic-mode analysis," *IEEE Antennas Wireless Propag. Lett*, vol. 22, no. 7, pp. 1677-1681, July 2023.

[12] C. Huang, C. -J. Guo, Y. Yuan and J. Ding, "Dual-band dual-sense high-gain circularly polarized metasurface antenna using characteristic mode analysis," *IEEE Antennas Wireless Propag. Lett*, vol. 22, no. 1, pp. 154-158, Jan. 2023.

[13] J. F. Gao and F. H. Lin, "Modeling and analysis of wideband multilayer metasurface antenna array using characteristic-mode analysis," *IEEE Trans. Antennas Propag.*,, vol. 71, no. 3, pp. 2832-2836, March 2023.

[14] A. El Yousfi, A. Lamkaddem, K. A. Abdalmalak and D. Segovia-Vargas, "A broadband circularly polarized single-layer metasurface antenna using characteristic-mode analysis," *IEEE Trans. Antennas Propag.*, vol. 71, no. 4, pp. 3114-3122, April 2023.

[15] K. R. Jha, N. Rana and S. K. Sharma, "Design of compact antenna array for mimo implementation using characteristic mode analysis for 5G NR and Wi-Fi 6 applications," *IEEE Open Journal of Ant and Propag*, vol. 4, pp. 262-277, 2023.

[16] W. Lin, R. W. Ziolkowski, and T. C. Baum, "28 GHz compact omnidirectional circularly polarized antenna for device-to-device communications in the future 5G systems," *IEEE Trans. Antennas Propag.*, vol. 65, no. 12, pp. 6904–6914, Dec. 2017.

[17] T. Rappaport, Y. Xing, G. R. MacCartney, A. F. Molisch, E. Mellios, and J. Zhang, "Overview of millimeter wave communications for fifth generation (5G) wireless networks-with a focus on propagation models," *IEEE Trans. Antennas Propag.*, vol. 65, no. 12, pp. 6213–6230, Dec. 2017.

[18] W. Hong, K.-H. Baek, and S. Ko, "Millimeter-wave 5G antennas for smartphones: Overview and experimental demonstration," *IEEE Trans. Antennas Propag.*, vol. 65, no. 12, pp. 6250–6261, Dec. 2017.

[19] Y. Yang, B. Sun, and J. Guo, "A low-cost, single-layer, dual circularly polarized antenna for millimeter-wave applications," *IEEE Antennas Wireless Propag. Lett.*, vol. 18, no. 4, pp. 651–655, Apr. 2019.

[20] U. Ullah, S. Koziel, and I. B. Mabrouk, "Rapid redesign and bandwidth/size tradeoffs for compact wideband circular polarization

antennas using inverse surrogates and fast EM-based parameter tuning," *IEEE Trans. Antennas Propag*., vol. 68, no. 1, pp. 81–89, Jan. 2020.

[21] C. Zhao and C.-F. Wang, "Characteristic mode design of wide band circularly polarized patch antenna consisting of H-shaped unit cells," *IEEE Access*, vol. 6, pp. 25292–25299, 2018.

[22] C. S. Lee, Y. Fan, and M. Ezzat, "Single-feed circularly polarized microstrip antenna with Bethe holes on the radiating patch," *IEEE Trans. Antennas Propag.*, vol. 68, no. 6, pp. 4935–4938, Jun. 2020.

[23] J. Zeng, X. Liang, L. He, F. Guan, F. H. Lin, and J. Zi, "Single fed triple-mode wideband circularly polarized microstrip antennas using characteristic mode analysis," *IEEE Trans. Antennas Propag*., vol. 70, no. 2, pp. 846–855, Feb. 2022.

[24] U. Ullah, M. Al-Hasan, S. Koziel and I. B. Mabrouk, "Series-slot-fed circularly polarized multiple-input–multiple-output antenna array enabling circular polarization diversity for 5G 28 GHz indoor applications," *IEEE Trans. Antennas Propag.*, vol. 69, no. 9, pp. 5607-5616, Sept. 2021

[25] Y.-M. Cai, K. Li, Y.-Z. Yin, and W. Hu, "Broadband circularly polarized printed antenna with branched microstrip feed," *IEEE Ant. Wireless Prop. Lett.*, vol. 13, pp. 674–677, 2014.

[26] S. Mohammadi-Asl, J. Nourinia, C. Ghobadi, and M. Majidzadeh, "Wideband compact circularly polarized sequentially rotated array antenna with sequential-phase feed network," *IEEE Antenna Wireless Propag. Lett.*, vol. 16, pp. 3176–3179, 2017.

[27] U. Ullah and S. Koziel, "A novel coplanar-strip-based excitation technique for design of broadband circularly polarization antennas with wide 3 dB axial ratio beamwidth," IEEE Trans. Ant. Prop, vol. 67, no. 6, pp. 4224-4229, June 2019.

[28] H. L. Zhu and S. W. Cheung, "Design of polarization reconfigurable antenna using metasurface," *IEEE Trans. Antennas Propag.*, vol. 62, no. 6, pp. 2891–2898, Mar. 2014.

[29] F. H. Lin and Z. N. Chen, "Low-profile wideband metasurface antennas using characteristic mode analysis," *IEEE Trans. Antennas Propag*., vol. 65, no. 4, pp. 1706–1713, Apr. 2017.

[30] S. Liu, D. Yang, Y. Chen, X. Zhang, and Y. Xiang, "High isolation and low cross-polarization of low-profile dual-polarized antennas via metasurface mode optimization," *IEEE Trans. Antennas Propag*., vol. 69, no. 5, pp. 2999–3004, May 2021.